

Detection of abundant solid CO in the disk around CRBR 2422.8-3423 [★]

W. F. Thi^{1,2}, K. M. Pontoppidan², E. F. van Dishoeck², E. Dartois³, and L. d'Hendecourt³

¹ Department of Physics and Astronomy, University College London, Gower Street, London WC1E 6BT, U.K.

² Leiden Observatory, P. O. Box 9513, 2300 RA, Leiden, The Netherlands

³ Astrochimie Expérimentale, Institut d'Astrophysique Spatiale, Université Paris-Sud, Bât. 121, F-91405 Orsay, France

Received ... ; Accepted ...

Abstract. We present direct evidence for CO freeze-out in a circumstellar disk around the edge-on class I object CRBR 2422.8-3423, observed in the M band with VLT-ISAAC at a resolving power $R \simeq 10\,000$. The spectrum shows strong solid CO absorption, with a lower limit on the column density of $2.2 \times 10^{18} \text{ cm}^{-2}$. The solid CO column is the highest observed so far, including high-mass protostars and background field stars. Absorption by foreground cloud material likely accounts for only a small fraction of the total solid CO, based on the weakness of solid CO absorption toward nearby sources and the absence of gaseous $\text{C}^{18}\text{O } J = 2 \rightarrow 1$ emission $30''$ south. Gas-phase ro-vibrational CO absorption lines are also detected with a mean temperature of 50 ± 10 K. The average gas/solid CO ratio is ~ 1 along the line of sight. For an estimated inclination of $20^\circ \pm 5^\circ$, the solid CO absorption originates mostly in the cold, shielded outer part of the flaring disk, consistent with the predominance of apolar solid CO in the spectrum and the non-detection of solid OCN^- , an indicator of thermal/ultraviolet processing of the ice mantle. By contrast, the warm gaseous CO likely originates closer to the star.

Key words. star formation – ISM: dust, extinction – molecules – abundances – Infrared: ISM: lines and bands

1. Introduction

Interstellar gas and dust form the basic ingredients from which planetary systems are built (e.g., van Dishoeck & Blake 1998, Ehrenfreund & Charnley 2000). In particular, the icy grains can agglomerate in the cold midplane of circumstellar disks to form planetesimals such as comets. In the cold ($T < 20$ K) and dense ($n_{\text{H}} = 10^6 - 10^9 \text{ cm}^{-3}$) regions of disks, all chemical models predict a strong freeze-out of molecules onto grain surfaces (e.g., Aikawa et al. 2002). The low molecular abundances in disks compared to those in dense clouds as derived from (sub)millimeter lines is widely considered to be indirect evidence for freeze-out (Dutrey, Guilloteau & Guélin 1997; Thi et al. 2001).

Observations of gaseous and solid CO have been performed for a few transitional objects from class I to class II that are known to possess a disk. Boogert et al. (2002a) observed L 1489 in Taurus – a large 2000 AU rotating disk –, but the amount of solid CO is not exceptionally high ($\sim 7\%$ of gaseous CO). This may stem from the fact that these systems are still far from edge-on (inclination $\sim 20^\circ - 30^\circ$) so that the line of sight does not intersect

the midplane, the largest reservoir of solid CO. Shuping et al. (2001) found strong CO depletion toward Elias 18 in Taurus, but both the disk structure and its viewing angle are not well constrained. More promising targets are pre-main-sequence stars for which near-infrared images have revealed nebulosities separated by a dark lane (e.g. Padgett et al. 1999). The lane is interpreted as the cold midplane of a disk seen close to edge-on where visible and even near-infrared light are extremely extinct. Among such dark-lane objects, CRBR 2422.8-3423 is a red ($H - K = 4.7$) low luminosity ($L = 0.36 L_{\odot}$, Bontemps et al. 2001) object surrounded by a near edge-on disk, discovered in images with the ESO *Very Large Telescope* (VLT) at $2 \mu\text{m}$ (Brandner et al. 2000). Its spectral energy distribution (SED) is consistent with that of a class I object or an edge-on class II object with strong silicate absorption at $9.6 \mu\text{m}$. It is located at the edge of the ρ Oph cloud complex in the core F, $\sim 30''$ west of the infrared source IRS 43 and a few arcmin south-east of Elias 29 (Motte, André & Montmerle 1998).

This letter reports the detection of a large quantity of solid CO and the presence of gaseous CO in the line of sight of CRBR 2422.8-3423 using the ESO-VLT (§2 and 3). Possible contamination by foreground cloud material is

[★] Based on observations obtained at the European Southern Observatory (ESO), Paranal, Chile, within the observing program 164.I-0605.

considered in § 4, followed by a discussion on the location and origin of the CO gas and dust in the disk (§5).

2. Observations

CRBR 2422.8-3423 was observed with the ESO VLT-ANTU mounted with the *Infrared Spectrometer And Array Camera* (ISAAC) on May 6, 2002. A spectrum at $R \approx 10^4$ was obtained in the M band using a slit-width of $0''.3$, which matched the excellent seeing ($\approx 0''.3$ at $4 \mu\text{m}$). The integration time was 36 minutes, resulting in a continuum S/N of ≈ 20 . The spectra of BS 6084 (B1III) and BS 6378 (A2.5Va), observed immediately before and after CRBR 2422.8-3423, were used to remove the atmospheric features and to calibrate the spectrum in flux and wavelength. All the reduction steps were carried out using an in-house data reduction package written in *IDL*.

Observations of gaseous CO (sub)millimeter lines on source and at an offset position $30''$ south were obtained at the *James Clerk Maxwell Telescope* (JCMT)¹ in June 2002. The dual-polarization receiver B3 was tuned to observe the $^{12}\text{CO } J = 3 \rightarrow 2$ (345.796 GHz, beam $13''.8$) and $^{13}\text{CO } J = 3 \rightarrow 2$ (330.587 GHz, beam $14''.4$) lines, and receiver A3 to obtain $\text{C}^{18}\text{O } J = 2 \rightarrow 1$ (219.560 GHz, beam $22''.2$). The backend was the Digital Autocorrelator Spectrometer, set at a resolution of $\sim 0.15 \text{ km s}^{-1}$. The beam efficiencies are $\eta_{\text{mb}}=0.63$ (345 GHz) and $\eta_{\text{mb}}=0.69$ (230 GHz). The fluxes were calibrated against the bright nearby source IRAS 16293-2422. The observations were acquired in position switching with a throw of $1800''$ south and reduced using the *SPECX* software.

3. Results and analysis

3.1. VLT-ISAAC spectrum

A saturated absorption feature centered at $\sim 4.67 \mu\text{m}$ and assigned to solid CO is seen in the M -band spectrum displayed in the upper panel of Fig. 1. No broad absorption at $4.62 \mu\text{m}$, usually attributed to solid OCN^- and a signpost of thermal and/or ultraviolet processing, is present, although the limit of $\tau \leq 0.05$ is not strong. Unresolved gas-phase CO lines are also detected. A continuum which takes into account absorption by silicate is fitted to the data. The continuum subtracted spectrum is shown in the lower panel of Fig. 1 in transmission scale.

The best fit to the saturated solid CO band is $\tau \approx 6.2$, corresponding to $N(\text{CO}_{\text{ice}}) \approx 2.2 \times 10^{18} \text{ cm}^{-2}$ using the integrated band strength of Gerakines et al. (1995). This is the highest solid CO column density found to date, even compared with ice-rich high-mass sources such as NGC 7538 IRS9 (e.g. Chiar et al. 1998, 1995). The solid CO profile toward CRBR 2422.8-3423 can be decomposed into

¹ The James Clerk Maxwell Telescope is operated by the Joint Astronomy Centre in Hilo, Hawaii on behalf of the Particle Physics and Astronomy Research Council in the United Kingdom, the National Research Council of Canada and The Netherlands Organization for Scientific Research.

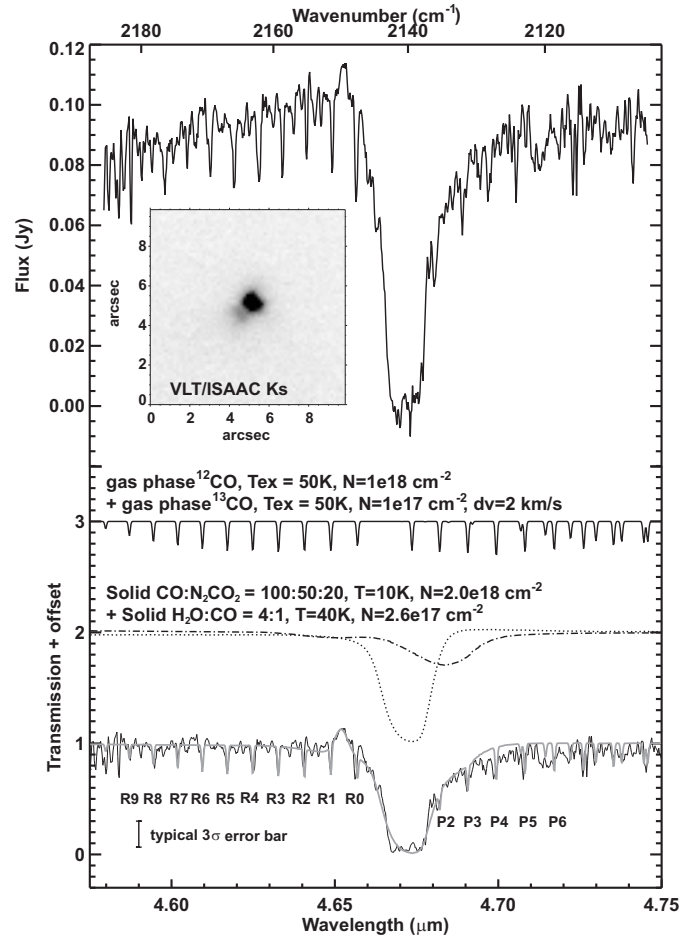


Fig. 1. VLT-ISAAC M band spectrum toward CRBR 2422.8-3423 (upper panel). The insert shows the VLT Ks image taken by Brandner et al. (2000). The upper curve of the lower panel shows the gas-phase model, convolved to the observed spectral resolution and shifted in wavelength to account for a source heliocentric velocity of 10 km s^{-1} . The middle curve displays laboratory absorption spectra of apolar (dotted) and polar (dashed) CO ice mixtures. The sum of the two models including Pfund β emission at $4.65 \mu\text{m}$ is overlaid on the observed spectrum in the bottom curve.

a narrow saturated component, usually ascribed to apolar CO in a H_2O -poor matrix, and a broad red wing at $4.685 \mu\text{m}$, indicative of polar CO in an H_2O -rich matrix. Using optical constants from the Leiden database including grain shape effects (Ehrenfreund et al. 1997), a χ^2 search for the best-fitting laboratory mixtures was performed. The saturation of the line prevents any unique fit, but the apolar CO is best matched by a mixture $\text{CO}:\text{N}_2:\text{CO}_2=100:50:20$ at 10 K with $N=2.0 \times 10^{18} \text{ cm}^{-2}$. The red-wing is fitted by $\text{H}_2\text{O}:\text{CO} = 4:1$ at 40 K with $2.6 \times 10^{17} \text{ cm}^{-2}$. The latter column density is comparable to that found toward L 1489, which has a luminosity of $3.7 L_{\odot}$. The large amount of apolar CO indicates low temperatures along the line of sight, since it evaporates around $\sim 20 \text{ K}$.

The VLT spectrum shows the presence of narrow gas-phase ^{12}CO and ^{13}CO ro-vibrational lines originating from levels up to $J = 9$ (250 K above ground). Synthetic LTE model spectra were fitted to the observed spectrum using data from the HITRAN database (Rothman et al. 1992). The fit parameters are the gas temperature T_{ex} , the column density $N_{\text{gas}}(\text{CO})$ and the velocity broadening ΔV , assumed to be smaller than 2 km s^{-1} from the JCMT data. The limited number and the high optical depth of the ^{12}CO lines prevent a unique fit, but the best result (see Fig. 1) is obtained for $T_{\text{ex}} = 40 - 60 \text{ K}$, which is probably a mean between the cold and warm components along the line of sight. The fit includes the ^{13}CO lines. The optical depth of the ^{12}CO lines is likely underestimated so that the gas-phase CO column density can range from 1 to $6 \times 10^{18} \text{ cm}^{-2}$. Adopting a mean value of $3 \times 10^{18} \text{ cm}^{-2}$, the line of sight average gas/solid CO ratio is ~ 1 . Comparing the column of gas-phase CO with that of polar solid CO only, the ratio drops to ~ 0.1 . The latter value is comparable to that found for L 1489 (0.07, see Boogert et al. 2002a) but still higher than for Elias 18 (0.01, Shuping et al. 2001). If the lines were significantly wider than 2 km s^{-1} as found for L 1489 ($\sim 20 \text{ km s}^{-1}$), the gaseous CO column density would drop by an order of magnitude.

3.2. JCMT spectra

The $\text{C}^{18}\text{O } J = 2 \rightarrow 1$ emission observed with the JCMT is shown in the upper panel of Fig. 2. Strong $^{12}\text{CO } J = 3 \rightarrow 2$ ($\sim 12 \text{ K}$ peak temperature) and $^{13}\text{CO } J = 3 \rightarrow 2$ ($\sim 7 \text{ K}$ peak temperature) lines are also detected, but are not displayed here since their profiles are similar to that of C^{18}O . $\text{C}^{18}\text{O } J = 2 \rightarrow 1$ is detected on source only. Compared with single-dish CO 3–2 and 2–1 lines from disks around older isolated pre-main-sequence stars in Taurus (e.g., Thi et al. 2001), the lines toward CRBR 2422.8-3423 are more than an order of magnitude stronger and do not show the double-peak profile resulting from the projection of a disk in Keplerian rotation. The CRBR 2422.8-3423 spectrum shows three peaks, two of which have velocities similar to those seen toward Elias 29 and interpreted as arising from the cloud ridge in which the source is embedded ($N(\text{CO}_{\text{gas}})_{\text{cloud}} \simeq 2.9 \times 10^{18} \text{ cm}^{-2}$, Boogert et al. 2002b). The total integrated $\text{C}^{18}\text{O } 2-1$ intensity on source is $13.6 \pm 4 \text{ K km s}^{-1}$. The corresponding ^{12}CO column density is $(0.5-1) \times 10^{19} \text{ cm}^{-2}$ assuming $T_{\text{ex}} = 15 \text{ K}$ (cf. Motte et al. 1998 for ρ Oph clump F) and $^{18}\text{O}/^{16}\text{O}=560$ (Wilson & Rood 1994). For $T_{\text{ex}} = 50 \text{ K}$, the column densities are lowered by 30%. The non-detection of $\text{C}^{18}\text{O } J = 2 \rightarrow 1$ at the offset position suggests a ^{12}CO column density less than $1 \times 10^{17} \text{ cm}^{-2}$ for $T_{\text{ex}} = 15 \text{ K}$, around 20 times lower.

4. Contamination by foreground material?

Absorption studies toward young stellar objects located in the ρ Oph cloud complex can be dominated by foreground cloud(s) (Boogert et al. 2002b). The SCUBA $850 \mu\text{m}$ map of ρ Oph by Johnstone et al. (2000) shows that CRBR

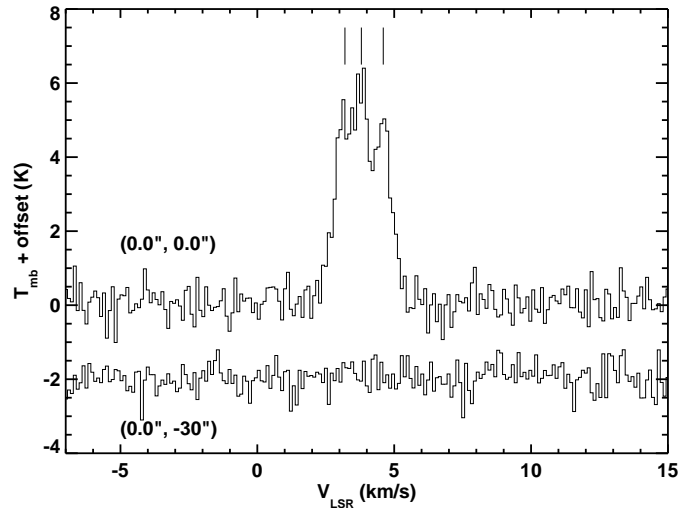


Fig. 2. $\text{C}^{18}\text{O } J = 2 \rightarrow 1$ obtained using the JCMT toward CRBR 2422.8-3423 on source (upper spectrum) and at an offset position $30''$ south (lower spectrum).

2422.8-3423 is indeed at the edge of the ridge which contains both Elias 29 and the nearby class I object IRS 43. The lack of CO emission at the offset position indicates however that the bulk of the gas-phase CO is located within 3000 AU from CRBR 2422.8-3423. The similarity of the gaseous CO column densities derived from the on-source $\text{C}^{18}\text{O } 2-1$ emission and the VLT-ISAAC infrared absorption may be fortuitous since the VLT-ISAAC data do not probe very cold CO with small ($\lesssim 1 \text{ km s}^{-1}$) line widths. We cannot exclude that part of the gas-phase CO seen in the infrared arises in a more extended envelope or cloud, but the fact that the CO excitation temperature is significantly above 10 K indicates that at least some fraction must originate close to the young star in a warm part of the disk.

For solid CO, there are strong arguments that most of the absorption must arise in the disk. The bright nearby ($\sim 30''$ east) source IRS 43 was observed simultaneously with CRBR 2422.8-3423 with VLT-ISAAC and has a CO ice optical depth of only 1.87 ± 0.02 , corresponding to $N(\text{CO}_{\text{ice}}) = 7 \times 10^{17} \text{ cm}^{-2}$ (Pontoppidan et al., in prep.). This is at least a factor of 3 lower than toward CRBR 2422.8-3423 even though its $850 \mu\text{m}$ flux is a factor of 1.5 higher. Toward Elias 29, solid CO has an optical depth of only 0.25, most of which is believed to be located in the foreground clouds. Compared to the optical depth found toward CRBR 2422.8-3423 ($\tau_{\text{ice}}(\text{CO}) \gtrsim 6$), this amount of foreground material can account for only an insignificant fraction of the observed solid CO. Finally, if clouds happen to lie in front of CRBR 2422.8-3423, the moderate extinction ($A_V < 10$) of those clouds probably prevents them to harbour significant amounts of solid CO (Shuping et al. 2000). Indeed, in a M -band survey of more than 30 young stellar objects, this is the deepest CO ice band observed.

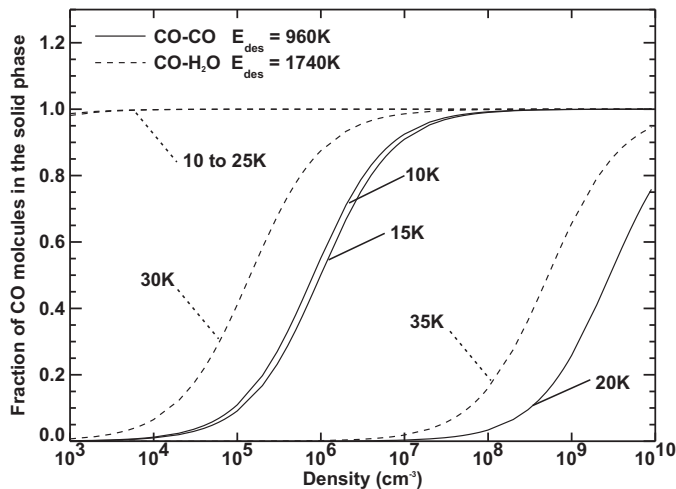


Fig. 3. Fraction of CO molecules in the solid phase at different temperatures as function of density. Adsorption onto H₂O and CO ice produce different results. The desorption energies are from Sandford & Allamandola (1988) for CO-H₂O and Sandford et al. (1988) for CO-CO.

5. Discussion

A simple disk model cf. Chiang & Goldreich (1999) with $T_* = 3500$ K and a disk radius of 250 AU has been adopted to investigate the location of the solid and gaseous CO seen in infrared absorption. Because of its higher temperature, the gaseous CO is likely not co-located with the bulk of the apolar solid CO, which evaporates at ~ 20 K. The polar solid CO can however reside in the same region of the disk as the CO gas at 40–60 K. Assuming that CO is frozen out at < 20 K (apolar CO) and < 40 K (polar CO), the best fit to the column densities, gas/solid CO and polar ice/apolar ice ratio is obtained for $i = 20 \pm 5^\circ$. This inclination is consistent with the flux asymmetry seen in the near-infrared image of Brandner et al. (2000). For such line of sight, most of the CO ice is located above the midplane in the outer disk, whereas the CO gas is found in the warm inner disk. Thus, the overall CO depletion could be significantly higher than the ratio of ~ 1 found here.

Several time-dependent chemical models were run to quantify the gas/solid CO ratios in different density and temperature regimes. The models simulate gas-phase chemistry, freeze-out onto grain surfaces and thermal as well as non-thermal evaporation. Cosmic-ray induced desorption is modeled as in Hasegawa & Herbst (1993), which may be an overestimate for large grains in disks (Shen et al., in prep.). The sticking coefficient was set at 0.3 to account for other non-thermal mechanisms (e.g., Schutte & Greenberg 1997) and photodesorption is assumed ineffective. At $T > T_{\text{evap}}$ thermal desorption dominates, whereas at $T < T_{\text{evap}}$ cosmic-ray desorption prevails. In the model, T_{evap} is 20 K for apolar CO ice ($E_{\text{des}} = 960$ K) and 40 K ($E_{\text{des}} = 1740$ K) for polar CO. To illustrate the effects of thermal and cosmic-ray induced desorptions, Fig. 3 shows the gas/solid CO ratio at chemical equilibrium. In cold

($T < 20$ K) but moderately dense ($10^4 - 10^5 \text{ cm}^{-3}$) regions of the disk around CRBR 2422.8-3423, only a small amount of CO is depleted onto grains in the apolar form, but much larger fractions $> 50\%$ can occur at higher densities ($\sim 10^6 - 10^8 \text{ cm}^{-3}$).

In summary, we detected a large amount of solid CO in the line of sight toward CRBR 2422.8-3423. The majority of this ice is likely located in the flaring outer regions of the edge-on circumstellar disk. Very high resolution ($R > 10^5$) near-infrared spectroscopy is needed to reveal the gaseous CO line profiles and thus their origin and the gas dynamics in the inner disk. Future submillimeter interferometer data can probe the velocity pattern and excitation conditions of the gas as functions of disk radius, whereas mid-infrared spectroscopy with, e.g., the *Space Infrared Telescope Facility* (SIRTF) will allow searches for other ice components, in particular solid CO₂.

Acknowledgements. WFT thanks PPARC for a postdoctoral grant to UCL. Astrochemistry in Leiden is supported by a Spinoza grant from the Netherlands Organization for Scientific Research (NWO) and a PhD grant from the Netherlands Research School for Astronomy (NOVA). We thank the ESO staff for their help during the observations, P. Papadopoulos for performing the JCMT observations and D. Johnstone for a blow-up of the SCUBA map of ρ Oph.

References

- Aikawa, Y., van Zadelhoff, G. J., Herbst, E., & van Dishoeck, E. F. 2002, *A&A*, 386, 622
- Boogert, A. C. A., Hogerheijde, M. R., & Blake, G. A. 2002a, *ApJ*, 568, 708
- Boogert, A. C. A., Hogerheijde, M. R., Ceccarelli, C., et al. 2002b, *ApJ*, 570, 723
- Bontemps, S., André, P., Kaas, A. A., et al. 2001, *A&A*, 372, 173
- Brandner, W., Sheppard, S., Zinnecker, H., et al. 2000, *A&A*, 364, L13
- Chiang, E. I., & Goldreich, P. 1999, *ApJ*, 519, 279
- Chiar, J. E., Adamson, A. J., Kerr, T. H., Whittet, D. C. B. 1995, *ApJ*, 455, 234
- Chiar, J. E., Gerakines, P. A., Whittet, D. C. B., et al. 1998, *ApJ*, 498, 716
- Dutrey, A., Guilloteau, S., & Guélin, M. 1997, *A&A*, 317, L55
- Ehrenfreund, P., Boogert, A. C. A., Gerakines, P. A., Tielens, A. G. G. M., & van Dishoeck E. F. 1997, *A&A*, 328, 649
- Ehrenfreund, P., & Charnley, S. B. 2000, *ARA&A*, 38, 427
- Gerakines, P. A., Schutte, W. A., Greenberg, J. M., & van Dishoeck, E. F. 1995, *A&A*, 296, 810
- Hasegawa, T. I., & Herbst, E. 1993, *MNRAS*, 261, 83
- Johnstone, D., Wilson, C. D., Moriarty-Schieven, G., et al. 2000, *ApJ*, 545, 327
- Motte, F., André, P., & Neri, R. 1998, *A&A*, 336, 150
- Padgett, D. L., Brandner, W., Stapelfeldt, et al. 1999, *AJ*, 117, 1490
- Rothman, L. S., Gamache, R. R., Tipping, R. H., et al. 1992, *J. Quant. Spectrosc. Radiat. Transfer.*, 48, 469
- Sandford, S. A., & Allamandola, L. J. 1988, *Icarus*, 76, 201
- Sandford, S. A., Allamandola, L. J., Tielens, A. G. G. M., & Valero, G. J. 1988, *ApJ*, 329, 498
- Schutte, W. A., & Greenberg, J. M. 1997, *A&A*, 317, L43

- Shuping, R. Y., Snow, T. P., Chiar, J. E., & Kerr, T. H. 2000, ApJ, 529, 932
- Shuping, R. Y., Chiar, J. E., Snow, T. P., & Kerr, T. H. 2001, ApJ, 547, L161
- Thi, W. F., van Dishoeck, E. F., Blake, G. A., et al. 2001, ApJ, van Dishoeck, E. F., & Blake, G. A. 1998, ARA&A, 36, 317
- Wilson, T. L., & Rood, R. T. 1994, ARA&A, 32, 191